Nonlinear Dynamics Final Project Write-up: Locally Forced Surface Waves

Steven Tarr[1], Ashley Barnes[2], Alejandro Escontrela[2]
[1]Submission author, [2]Group members

Submitted December 8, 2020

1 Introduction

A recent fascination in nonlinear dynamics has been systems with locally oscillating interactors [1–3]. The local wave-like components of these systems have been the source of novel dynamical interactions, with one particularly striking example being the "diffraction" phenomenon seen in the scattering of a snakelike robot off a series of posts [2]. In search of related cutting-edge phenomena, it is a natural logical step to recontextualize the local oscillations into the waves of a fluid system. While nonlinear phenomena in globally oscillated fluid systems have been studied extensively in laboratory settings [4–8] and theoretical and numerical contexts [9–11], locally excited systems have gone largely untouched and may reveal unique dynamics owing to the additional spatial parameters. While global vibration studies provide an excellent foundation for their ease of control and reduced parameter spaces, fluid and fluid-like systems with local oscillations are more easily motivated by natural settings and are particularly relevant in physics of living systems [1, 12] and aquatic technology contexts [13, 14]. We began our investigation by looking at a simple system consisting of a vibrating intruder sending surface waves across a cup of water. During this preliminary excursion, we observed frequency and intrusion depth thresholds within which the generated waves possessed some visual similarities to Faraday waves, a thoroughly studied fluid phenomenon which we now briefly explain.

First described by Michael Faraday in his seminal 1831 paper, Faraday waves are a nonlinear resonance phenomenon in fluid systems owing to parametric pumping above a certain acceleration threshold called the Faraday instability [4–11]; the specific threshold is determined by parameters intrinsic to the fluid such as viscosity, elasticity, and spatial dimensions [6, 8, 10]. When the whole system is subjected to vertical oscillations above this instability, the fluid surface becomes unstable to standing waves, resulting in surface waves that oscillate at the first subharmonic – precisely one half – of the driving frequency [5, 8, 9]. The subharmonic fluid oscillation is rationalized as a modulation of the system's acceleration due to gravity. To account for the parametric pumping, the typical gravity term in the Mathieu equations for amplitudes of fluid wave eigenmodes is replaced with an effective gravity term given by the sum of the original term and a cosine; the new ground state solution of the modified equations is half the driving frequency [5, 6].

Depending on specific parameters of the fluid and the driving force, Faraday waves can exhibit many

complex shapes including stripes, squares, hexagons, and even higher fold symmetries [8, 10, 11], as well as states with multiple wave structures separated into distinct regions [7]. Inspired by the evocative striped and cross-wave patterns observed in preliminary exploration, we set out to better understand the nature of locally forced surface waves by investigating the effects on wave morphology of spatial parameters unique to a locally excited system as well as parameters shared by globally excited systems. In performing this foundational study on locally forced surface waves, we also aim to uncover the nature of the initial visual resemblance to Faraday waves and to see if such a comparison has any real credence.

2 Methods

2.1 Experimental Apparatus

To investigate the types of surface waves produced by local oscillatory forces, we assembled a set of experimental apparatus; due to the coronavirus pandemic, each group member built their own separate apparatus seen in Fig. 1. Though the specifics of each apparatus varied with individually available resources, a set of common methods were employed by each member: (1) A 6"-inner-diameter circular plastic takeout container was filled with tap water to height 50 mm and affixed at the bottom to a flat surface. (2) A 3D-printed flat-end piston of length 50 mm was attached to the diaphragm of an EWA A106 Bluetooth speaker with rubber cement. Pistons were fabricated with three possible faces (circle, square, triangle) and four possible radii (5, 10, 15, 20 mm); for each circle radius, the inscribed square and equilateral triangle were used. (3) The piston-speaker assembly was suspended over the center of the container by a rigid stand that permitted variation of piston submersion depth. (4) To generate the requisite waves for study, the speaker was connected to a function generator application (f Generator V5.4.1, Thomas Gruber, EE-Toolkit.com) to drive the piston with specified waveforms. For consistency, all experiments used sine waves at the maximum amplitude allowed by the function generator.

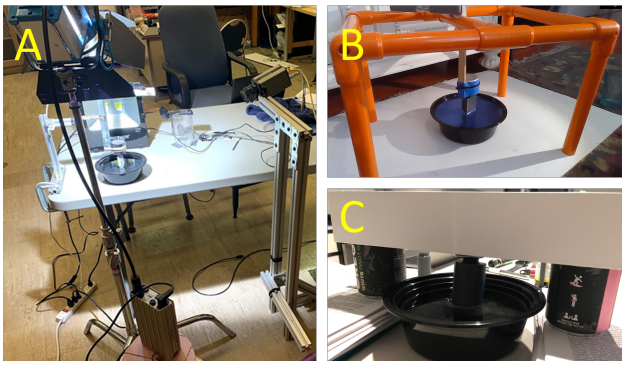

FIG. 1: *Three apparatus for studying locally forced surface waves. As a result of the coronavirus pandemic, experiments were performed in three separate locations. (A) was employed by Tarr, (B) by Barnes, and (C) by Escontrela.*

Each member recorded videos at 30 FPS with a smartphone camera or webcam mounted at an oblique angle. The Tarr apparatus (Fig. 1A) had access to an AOS Technologies S-Motion high-speed camera to record videos at 450 FPS. A clear distinction will be made between data extracted from high-speed videos and any other camera. The clarity afforded by high-speed videos of waves enables additional analysis that was not permitted by other cameras.

2.2 System Parameters

As a consequence of studying locally forced waves, we highlight a set of parameters unique to our locally driven apparatus when compared with traditional globally driven surface wave investigations, including piston submersion depth and piston geometry. We also draw connections to existing studies on globally driven fluid systems through common parameters like driving frequency and fluid viscosity. For each of the following studies, we repeated the described experimental methods with piston submersion depths of 0 (flush with the waterline), 10, 20, 30, and 40 mm and a variety of driving frequencies between 20 and 120 Hz.

2.2.1 Piston Shape

We compare the resultant wave morphologies for pistons of a single radius (20 mm) with three different face shapes. We also briefly explore the flow field symmetries that result from concentric waves of these shapes. We visualize these flow fields by adding sparse particulate matter to the fluid surface.

2.2.2 Piston Radius

We isolate the three piston face shapes and compare the resultant wave morphologies for pistons of a single shape with four different radii. We establish a connection between the two types of variation in piston geometry (shape and radius) through piston cross-sectional area.

2.2.3 Fluid Viscosity

We repeat the above studies on the effects of piston geometry with a layer of extra-fine (estimated 250-350 micron polydisperse) glitter covering the entire water's surface when unperturbed. In comparing the tests with glitter to those without, we study how a change in effective fluid viscosity affects resultant wave morphologies.

2.2.4 Excited Wave Frequency

Though the simplicity of the apparatus made quantitative measurements impractical, the high-speed videos enable a brute force method of counting frames to determine the frequency of excited waves. We employ this method to analyze videos of the most complex wave morphologies exhibited throughout the above three studies and compare the fixed driving frequency of the piston to both the frequency of the simple concentric waves excited before steady state and the frequency of the complex steady state waves. We verify the consistency of wave frequency by averaging over 5 periods at multiple container locations and video timestamps. We compare the observed frequencies to the established theory of Faraday waves.

2.2.5 Container Vibrational Damping

In response to an observation that the rim of the plastic container shakes significantly for some above experiments, we replace the plastic container with a metal mixing bowl filled with water to the same 50 mm

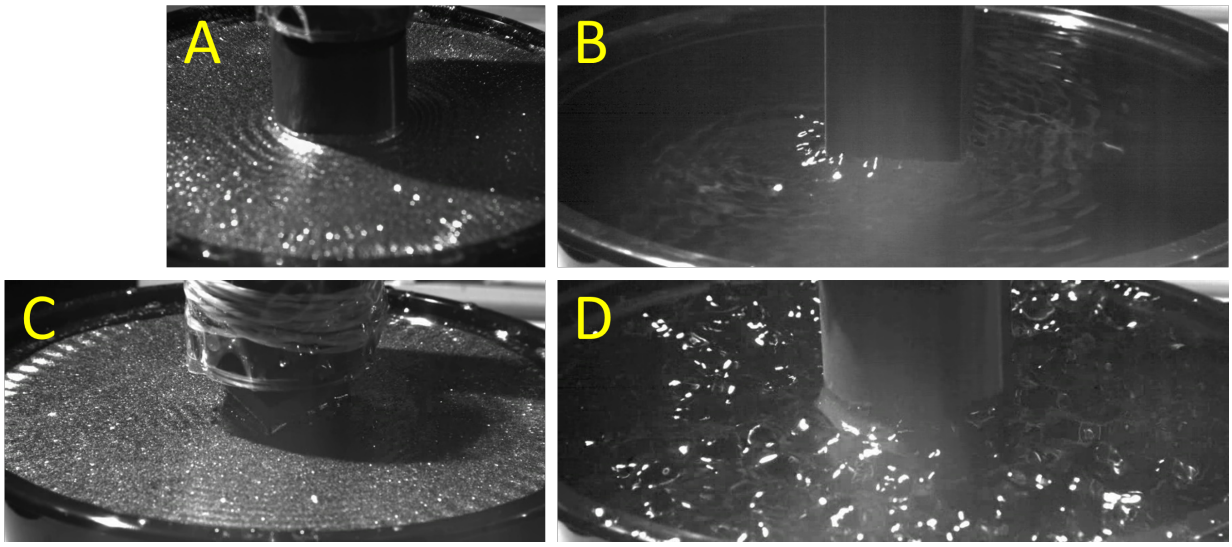

FIG. 2: *Archetypal examples of the four observed wave morphologies: (A) concentric waves, (B) interference pattern, (C) mixed state, and (D) bubbly waves.*

height. To further restrict container resonance, we add three 1 kg masses to the rim of the bowl at equal spacing. We compare the resultant wave morphologies for the weighted and unweighted metal bowls.

3 Results

In lieu of quantitative measurement, we start by establishing a qualitative taxonomy of observed wave morphologies that we use to better understand the effects of the many parameter variations described above. Throughout all performed experiments, the many emergent wave patterns broadly fell into four categories (see Fig. 2) that we define in order of increasing complexity: (1) "Concentric waves" refer to waves that mimic the shape of the piston at the waterline and expand outward without losing said shape. (2) "Interference patterns" refer to patterns of traveling waves that cannot be described by the motion of one easily identified waveform like a concentric wave and instead are owed to the superposition of more than one wave. (3) "Mixed states" refer to wave states that demonstrate two or more behaviors coexisting in visually distinct domains. In all trials with mixed states, we observed a central region of either concentric or interference waves with a ring of either standing or traveling striped waves aligned orthogonally to the boundary of the container. We derive the name "mixed state" from similar patterns that have been documented in studies of globally oscillated Faraday waves [7, 8]. (4) "Bubbly waves" refer to waves that exhibit complex structures that cannot be characterized in one dimension. These waves may be standing, traveling, or some superposition of the two. The qualities of a mixed state may accompany bubbly waves, but the converse is not true. The wave patterns often bear qualitative resemblance to globally forced Faraday waves, but without complete proof that our observed waves are indeed related to Faraday waves, we air on the side of caution and name our waves "bubbly" after an ostensible likeness to the memory of boiling water.

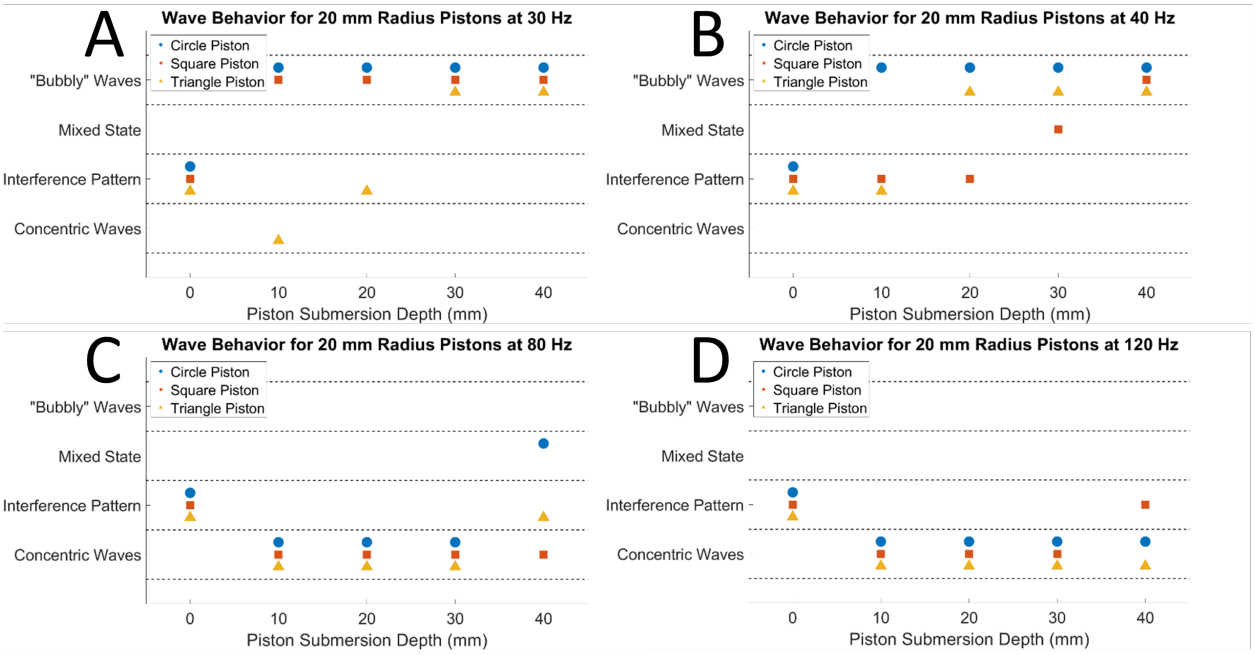

FIG. 3: *Wave morphology as a function of piston submersion depth and shape for driving frequencies (A) 30 Hz, (B) 40 Hz, (C) 80 Hz, (D) 120 Hz. All data were the result of high-speed video analysis. For lower frequencies, the circle piston quickly reaches highly complex waves as depth increases, with the square and triangle following shortly after. For higher frequencies, all shapes tend to concentric waves as depth increases.*

3.1 Piston Shape

For experiments at lower frequencies within the 20 to 120 Hz range tested, we typically observed an increase in wave complexity with increasing piston submersion depth (Fig. 3A, B). The circle piston often first generated bubbly waves at low submersion depths and maintained wave complexity for increased depth, while the square and triangle pistons tended to first generate bubbly waves at medium or large depths. As the driving frequency was increased, however, all three shapes generated waves of decreased complexity at all but the most extreme of tested depths (Fig. 3C, D). We reason that the driving amplitude of the speaker falls off at higher frequencies due to limitations of the voice coil mechanism; the reduced-amplitude vibrations force less water per unit time, resulting in less complex waves in the absence of potential boundary effects at either extreme of submersion depth.

In using sparse particulate matter to visualize the different flow fields for different piston shapes, we observed a 6-fold symmetry generated by the triangle piston and an 8-fold symmetry by the square piston. In both cases, water was ejected from the flat sides of the piston, circulated in a petal-like trajectory, and returned to the piston at the corner nearest to the ejection position. We explain the attraction to corners as a result of the sharp change in the curvature of the fluid meniscus. In their experiments on amphiphilic interactions due to the Cheerios effect, Cavallaro et al. show both experimentally and through numerical evaluation of the linearized Young-Laplace equation that buoyant particles experience an intense attraction to regions of a concave meniscus with high curvature, notably the corners of a square post [15]. We suspect the buoyant particulate matter in our system experiences the same attraction to the corners of the triangle

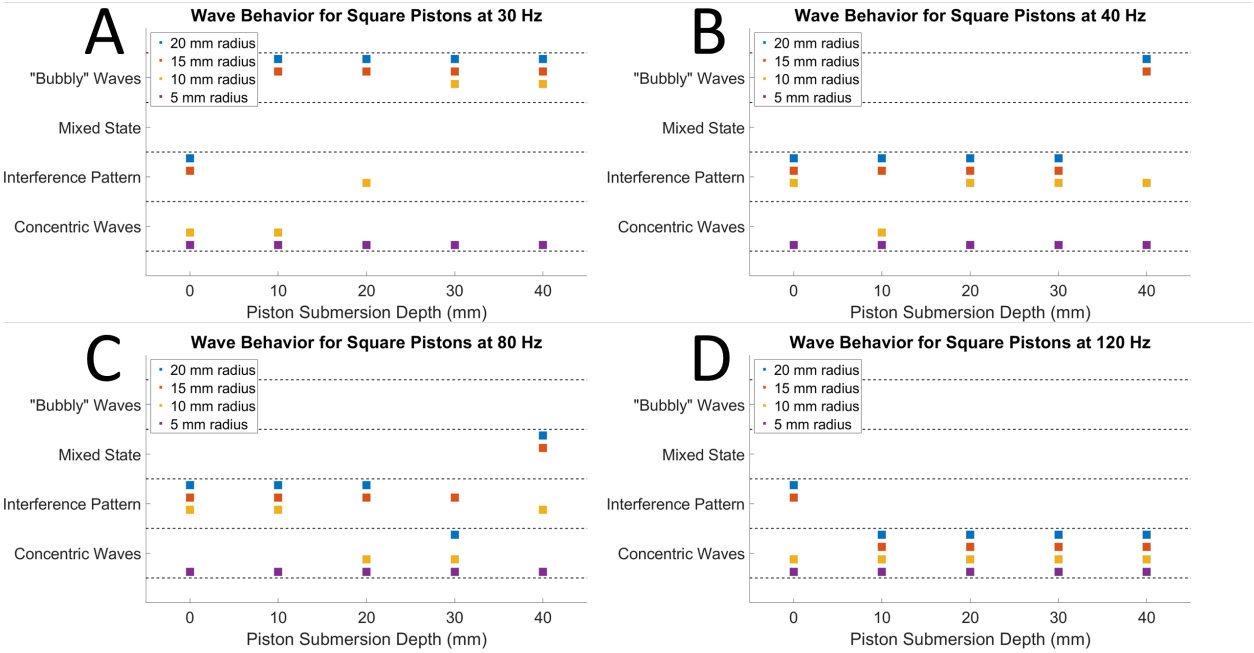

FIG. 4: *Wave morphology as a function of piston submersion depth and radius for driving frequencies (A) 30 Hz, (B) 40 Hz, (C) 80 Hz, (D) 120 Hz. All data were the result of webcam video analysis. Though the effects of submersion depth on wave morphology were not precisely reproduced in experiments with circle and triangle pistons of different sizes (not pictured), the decrease in wave complexity for higher driving frequencies and smaller piston sizes was recapitulated. Any other inconsistencies can be attributed to differences in both the experimental apparatus and environment due to the coronavirus pandemic.*

and square pistons. In contrast, the circle piston did not generate a recognizable symmetry; it instead displayed a few large petals spanning the container boundary with smaller sub-petals and vortices closer to the piston. Without high-curvature corners to drive the flow field generation, the circle piston yields a flow with less easily identifiable order.

3.2 Piston Radius

In experiments at all tested frequencies, we observed that pistons with smaller radii were much more likely to generate simple wave structures, with all 5 mm pistons generating only concentric waves for all tested submersion depths. For pistons with larger radii, we observed similar effects to trials with different shapes: lower frequency experiments often saw waves increase in complexity with submersion depth (Fig. 4A, B) while higher frequency experiments often saw waves decrease in complexity with depth (Fig. 4C, D). For a wide variety of depths and frequencies, an increase in piston radius corresponds to an increase in wave complexity.

FIG. 5: *Wave morphology as a function of piston submersion depth and (A, B) shape or (C, D) radius for trials (B, D) with and (A, C) without a layer of glitter atop the water's surface. All data were the result of high-speed video analysis. The glitter effectively increases the fluid viscosity and resists generation of highly complex waves.*

3.3 Fluid Viscosity

Though the decision to add a layer of glitter to the fluid surface originally came about as a wave visualization tool, we observed that experiments with otherwise identical parameter choices often demonstrated different wave morphologies upon the addition of glitter. We include a small selection in Fig. 5 of results directly comparing observed differences between setups with and without glitter when studying the differences between piston shapes (Fig. 5A, B) and radii (Fig. 5C, D). The addition of glitter often increased the necessary submersion depth for a fixed frequency piston to generate bubbly waves. When perturbed by waves, the glitter particles tended to stay clumped together and resist the forces trying to deform the surface into complex waves, implying that the addition of glitter can be treated as an effective increase in the fluid viscosity.

3.4 Excited Wave Frequency

High-speed analysis of trials demonstrating either a mixed state or bubbly waves with or without glitter reveals that the system always initiates with concentric waves and evolves to a complex steady state in roughly one second. We show the excited wave frequencies well before and during steady state in Fig. 6. In the early stages of forcing before the concentric waves start to evolve, we find that the waves consistently have frequency within 8.7% of the driving frequency for trials without glitter and within 10.% for trials with glitter, though both drop to within 2.3% when statistical error is accounted. Once a steady state is reached, we find that the waves have frequency within 8.5% of half the driving frequency for trials without glitter and within 4.2% of half the driving frequency for trials with glitter; again, both drop to within 1.0% and 0.0% respectively when statistical error is accounted. We verified the matching of the wave frequency

to the driving frequency for concentric waves that did not evolve in time. Additionally, we found that the concentric waves in the central region of the container during the generation of some mixed states oscillated with frequency very close to the driving frequency, while the striped waves at the container boundary during the generation of all mixed states oscillated with frequency very close to half the driving frequency.

3.5 Container Vibrational Damping

In experiments with the unweighted metal bowl, we found the waves generated to be similarly complex to the equivalent parameter choices with the plastic container. Upon the addition of the masses to damp the bowl vibration, the bubbly waves were often replaced with either interference patterns or concentric waves. The effect was most noticeable when the masses were added or removed mid-experiment, typically causing a sudden shift between complex wave morphology and concentric waves.

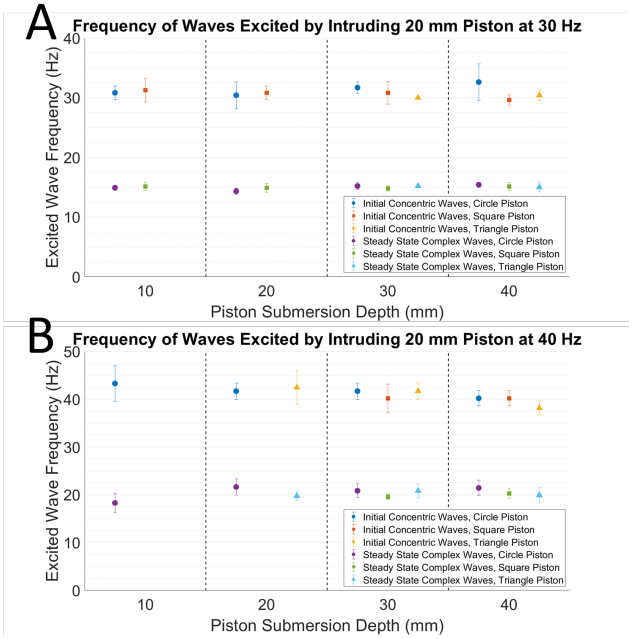

FIG. 6: *Frequencies of locally excited surface waves well before and during steady state driven at (A) 30 Hz and (B) 40 Hz. All data were the result of high-speed video analysis. Only trials that demonstrated bubbly waves or mixed states were included; any combination of piston shape and depth that appears to be missing corresponds to a trial that did not demonstrate bubbly waves or mixed states. Data were averaged over 5 periods taken at multiple locations and times to verify consistency. Analysis of equivalent experiments with glitter capture the same results.*

4 Discussion and Future Work

4.1 On Piston Geometry

When considering the similarities between resultant wave morphologies for tests on the effects of piston shape and radii, it bears stating that fixing the four radii of each piston shape to be equal resulted in a difference in piston cross-sectional area for the three shapes. For a fixed radius, the inscribed square and equilateral triangle have areas approximately 64% and 41% that of the circle respectively. We check the claim that cross-sectional area is a geometric parameter to unify results from shape and radius experiments by comparing the wave morphologies due to the two pistons closest in area – the 20 mm triangle and 15 mm square pistons (difference of roughly 70 mm^2). Indeed, we find that the resultant wave morphologies match for 17 out of the 20 combinations of frequency and depth tested (combinations shown in Figs. 3 and 4), further experimental evidence of area as a valuable parameter.

Though pistons of larger cross-sectional area will indeed displace more water with each period of oscillation leading to greater wave complexity, it would be foolish to overlook the tangible effects of different boundary conditions, which are most apparent when viewing near-piston concentric wave fronts and flow

field symmetries. We suggest two future experiments to further inspect the importance of these geometric piston parameters. First, revisiting the studies of piston shape and radii with pistons normalized by cross-sectional area rather than radius will serve to test the significance of piston area more thoroughly. Second, an experiment in which waves are globally excited while a piston of variable shape is held steady at various submersion depths will illuminate the effect that localized boundaries have on surface waves.

4.2 On Fluid Viscosity

For a particularly enlightening theoretical assessment of the effect of fluid viscosity on globally oscillated Faraday waves, we turn to Chen & Viñals's detailed derivations [10]. They show that high viscosity fluids prefer to form striped wave patterns while low viscosity fluids prefer more complex square and hexagonal patterns depending on the driving frequency. The results of experiments by Kudrolli & Gollub [7] compare favorably to Chen & Viñals's theory in their Fig. 1 [10]. Our observations for locally forced surface waves with a layer of glitter capture the same essence of decreasing wave complexity with increasing effective fluid viscosity as demonstrated in existing theory and experiment. Furthermore, the established shift to striped waves at higher viscosities matches nicely with the greater prevalence of mixed states in our experiments with glitter compared to those without glitter. Though we cannot be certain that our locally driven system displayed Faraday waves, the parallel effects of increased viscosity in both locally and globally excited systems suggests a possible connection be explored. To further validate the analogous fluid viscosity effect, we suggest revisiting our studies on the differences between the presence and absence of glitter with a set of homogeneous fluids of varying viscosities used in past Faraday wave studies such as silicone oil [5, 7], paraffin oil [6], and milk [4].

4.3 On Excited Wave Frequency

As described in the Introduction, a major distinguishing characteristic of Faraday waves is that the surface waves necessarily oscillate at half the driving frequency [4–11]. In showing that our concentric surface waves oscillate within 2.3% of the driving frequency and that both our bubbly waves and waves in the striped boundary region of our mixed states oscillate within 2.3% of half the driving frequency, we establish a strong connection between our system of locally driven surface waves and the globally driven Faraday waves. Additionally, the verification that our mixed states contain waves with frequency half of driving, the observation that the striped wave characteristics of our mixed states appear in some bubbly wave trials, and the above discussion on the prevalence of our mixed states in a higher viscosity fluid suggest that our mixed states are actually the simplest instance of bubbly waves. In addition to the examples given in the viscosity discussion, a qualitative resemblance exists between our mixed state waves and certain Faraday wave patterns created in laboratory experiments by Sheldrake & Sheldrake, most notably in Fig. 18b [8]. To probe the connection to Faraday waves further, we suggest employing more sophisticated data processing methods on videos with a wider range of driving frequencies to obtain a more rigorous and consistent analysis of the wave frequencies excited by local forcing.

4.4 On Container Vibrational Damping

Though we have heretofore discussed evidence to suggest a connection between our locally driven surface waves and traditional globally driven Faraday waves, we must also give space to results that suggest the contrary. When viewing high-speed videos of our experiments, it becomes apparent that while the base of the container is fixed, the rim is free to deform and shake in response to the pumping of the contained fluid, even in trials with the more rigid metal bowl. In trials with high wave complexity, the rim of either the plastic or metal container can be seen undergoing especially vigorous vibrations. However, when the allowed vibrations are damped by weighting the rim of the bowl, we observed a stark decrease in wave complexity. These results suggest the possibility that any semblance of Faraday waves in our experiments was not due to the local forcing of the piston, but instead due to a global parametric pumping from the resonant behavior of the container.

The conditions of the container have additional unintended and undesired effects in generating what Douady and Bechhoefer call meniscus waves [5, 6]. When the meniscus length at a boundary changes in response to a change in fluid height, a surface wave with frequency matching that of driving is emitted from the boundary to preserve fluid mass [5]. We observe these waves in our system most clearly at the very start of high-speed videos of trials with bubbly waves. In many cases, concentric waves can be seen emanating from the boundary before any concentric waves have traveled from the piston to the boundary; these waves may be attributed to either Douady's meniscus waves or the shaking of the container. Container vibrations and meniscus waves both create undesirable waves that muddy the results of our local forcing studies. We suggest improving the apparatus with more rigorous container vibrational damping; we also relay suggestions from papers by Douady and Bechhoefer to use brimful fluid conditions in a container made of or treated with a non-wetting material [5, 6].

5 Conclusion

In summary, we presented a detailed experimental investigation of the complexity of wave morphologies generated by local oscillatory forcing. We showed an increase in wave complexity with increased source submersion depth for low frequencies and a decrease in complexity for high frequencies. We reported an increase in wave complexity for pistons of larger cross-sectional area due to a change in face shape or radius. We discovered that increased fluid viscosity causes decreased wave complexity and paralleled this effect to those observed in prior Faraday wave studies. We showed that our simplest excited waves have frequency closely matching the driving frequency and that our most complex excited waves have frequency closely matching half the driving frequency, establishing a solid connection between the waves we observed and Faraday waves. Finally, we revealed the unintended presence of meniscus waves and the decrease in wave complexity when the fluid vessel is damped to vibrations. Though somewhat inconclusive due to shortcomings of our apparatus, our results hint at a rich phenomenology of locally excited surface waves with tangible connections to Faraday waves primed for further study.

6 Acknowledgments

I personally thank Ashley Barnes and Alejandro Escontrela for their dedicated efforts in data collection and analysis and for insightful discussions. I thank Professor Daniel I. Goldman, Enes Aydin, TA Christopher Crowley, and members of the CRAB Lab for support and advice both technical and analytical in nature.

References

[1] Maladen, R., Ding, Y., Li, C. & Goldman, D. I., "Undulatory swimming in sand: Subsurface locomotion of the sandfish lizard," *Science* **325**, 5938, 314–318 (2009).

[2] Rieser, J. M., Schiebel, P. E., Pazouki, A., Qian, F., Goddard, Z., Wiesenfeld, K., Zangwill, A., Negrut, D. & Goldman, D. I., "Dynamics of scattering in undulatory active collisions," *Phys. Rev. E* **99**, 022606, 1–13 (2019).

[3] Li, S., Aydin, Y. O., Small, G., Xiao, C., Rieser, J. M., Gynai, H. N., Laguna, P. & Goldman, D. I., "Self-propulsion on spandex: toward a robotic analog gravity system," 1–43 (2020), at <http://arxiv.org/abs/2004.03549>.

[4] Faraday, M., "On a peculiar class of acoustical figures; and on certain forms assumed by groups of particles upon vibrating elastic surfaces," *Philos. Trans. R. Soc. London* **121**, 1831, 299–340 (1831).

[5] Douady, S., "Experimental study of the Faraday instability," *J. Fluid Mech.* **221**, 5, 383–409 (1990).

[6] Bechhoefer, J., Ego, V., Manneville, S. & Johnson, B., "An experimental study of the onset of parametrically pumped surface waves in viscous fluids," *J. Fluid Mech.* **288**, 325–350 (1995).

[7] Kudrolli, A. & Gollub, J. P., "Localized spatiotemporal chaos in surface waves," *Phys. Rev. E - Stat. Physics, Plasmas, Fluids, Relat. Interdiscip. Top.* **54**, 2, 1052–1055 (1996).

[8] Sheldrake, M. & Sheldrake, R.,"Determinants of Faraday Wave-Patterns in Water Samples Oscillated Vertically at a Range of Frequencies from 50-200 Hz," *WATER J.* **9**, 1–27 (2017).

[9] Miles, J. & Henderson, D., "Parametrically Forced Surface Waves," *Annu. Rev. Fluid Mech.* **22**, 1, 143–165 (1990).

[10] Chen, P. & Viñals, J., "Amplitude equation and pattern selection in Faraday waves," *Phys. Rev. E - Stat. Physics, Plasmas, Fluids, Relat. Interdiscip. Top.* **60**, 1, 559–570 (1999).

[11] Périnet, N., Juric, D. & Tuckerman, L. S., "Numerical simulation of Faraday waves," *J. Fluid Mech.* **635**, 1–26 (2009).

[12] Moriarty, P. & Holt, R. G., "Faraday waves produced by periodic substrates: Mimicking the alligator water dance.," *J. Acoust. Soc. Am.* **129**, 4, 2411–2411 (2011).

[13] O'Hara, I., Paulos, J., Davey, J., Eckenstein, N., Doshi, N., Tosun, T., Greco, J., Seo, J., Turpin, M., Kumar, V. & Yim, M., "Self-assembly of a swarm of autonomous boats into floating structures," in *Proc. - IEEE Int. Conf. Robot. Autom.* 1234–1240 (2014).

[14] Shen, Y., Greco, M. & Faltinsen, O. M., "Numerical study of a well boat operating at a fish farm in long-crested irregular waves and current," *J. Fluids Struct.* **84**, 7491, 97–121 (2019).

[15] Cavallaro, M., Botto, L., Lewandowski, E. P., Wang, M. & Stebe, K. J., "Curvature-driven capillary migration and assembly of rod-like particles," *Proc. Natl. Acad. Sci. U. S. A.* **108**, 52, 20923–20928 (2011).